ICAS 2021 SHANGHAI
International Council of the Aeronautical Sciences
32nd Congress of the International Council of the Aeronautical Sciences
September 6-10, 2021
Pudong Shangri-La, Shanghai, China

PROGRESS OF BLENDED-WING-BODY AIRCRAFT DEVELOPMENT AT NORTHWESTERN POLYTECHNICAL UNIVERSITY

Zhenli Chen[1], YingChun Chen[2], Shuai Zhang[3], Lixin Wang[4], Zhaoguang Tan[2], Bao Chen[5], Shuwang Zhao[6], Long Wang[7], Jie Li[1], Changsheng Yuan[1], Yongjie Zhang[1], Yizhe Zhang[1], Weimi Sang[1], Yujin Tao[1], Dong Li[1] and Binqian Zhang[1]

[1]School of Aeronautics, Northwestern Polytechnical University, Xi'an 710072, China
[2]Shanghai Aircraft Design and Research Institute, COMAC, Shanghai 201210, China
[3]Beijing Aeronautical Science & Technology Research Institute (BASTRI), COMAC, Beijing 102211, China
[4]School of Aeronautic Science and Engineering, Beihang University, Beijing 100083, China
[5]AVIC Aerodynamics Research Institute, Ha'erbin 150001, China
[6]AVIC The First Aircraft Institute, Xi'an 710089, China
[7]AVIC Huiyang Aviation Propeller Co., LTD., Baoding 071051, China

Abstract

The blended-wing-body concepts were pursued in the last decades around the world to satisfy the projected demands of future green and sustainable aviation. A persistent effort of Northwestern Polytechnical University and the recent progress were summarized in the present paper. These efforts were supported by institutes and companies, including multidisciplinary design and optimization, stability and control design, propulsion and airframe integration, the noise shielding effects, cabin arrangements and egress, wind-tunnel experiments and modeling flight tests. A stable, high efficient, and safe design can be realized. However, much more work have to be done on the structure design and high-speed modeling flight test.

Keywords: Blended-wing-body concept, sustainable aviation, multidisciplinary design and optimization, noise shielding, modeling flight test

1. Introduction

The projected demand of future aviation poses the long-term challenges in efficiency, safety and environmental sustainability [1]. The classical swept tube-and-wing (TAW) configuration has been well optimized to the architecture's limit, which follows the Cayley's design principle. Therefore, it is essential to limit and to reduce environment impact of aviation by introducing new highly-efficient aircrafts and adopting advanced low-emission technologies.

Several unconventional configurations were investigated including truss-braced wing, box-wing, C-wing, flying wing, double-bubble lifting fuselage and blended-wing-body (BWB). The BWB concept was promoted to achieve distinct aerodynamic efficiency during cruise phase. This configuration can reduce form drag by increasing wetted aspect ratio, increase spanwise efficiency by using lifting fuselage, and reduce the interference drag by smoothly blended the wing and the body [2]. By the studies of the past decades, it is shown that the BWB configuration has the potential to simultaneously fulfill requirements on low fuel consumption and emissions. Despite great efforts have been made in United States of America, Russia and European countries, there are still enormous challenges that need to be resolved [2]-[4].

Table 1 Projects of NPU on BWB development [3]

Year	Project	BWB	*Payload*	*Range[nm]*	*Mach*	Experiments
2008-10	C919-B	BWB-150	150	3000	0.78	No
2014	SWB	BWB-300	300	7000	0.82	Low speed
2017	BWB	BWB-330	330	7500	0.85	Low/High speed

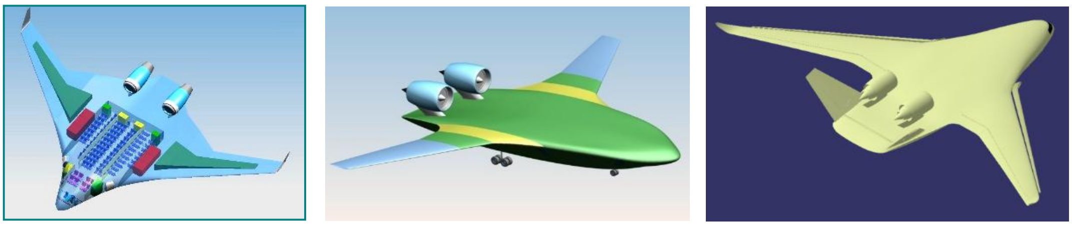

(a) BWB-150 (b) BWB-300 (c) BWB-330

Figure 1 Three BWB configurations developed at NPU

Most of the BWB studies were performed in the academia in China [5]-[11]. A systematically study were performed over the past decade under the cooperation of universities, research institute and industry, as shown in Table 1 [3]. The Comercial Aircraft Corporation of China (COMAC) started the conceptual design of C919 in 2008. A BWB concept named BWB-150 was systematically investigated by Northwestern Polytechincal University (NPU) in corporation with COMAC from 2008 to 2010, as shown in Figure 1(a). The cargo payload was arranged between the outboard wing and the center pressurized cabin to resolve the constrains on the cabin height. An aircraft-level benefit of 15% was achieved compared with the conventional TAW under the same technology assumptions.

A subsequent project was funded on BWB design to resolve the challenges under the constrains of cruise performance until 2014. A BWB configuration was projected to satisfy the requirements of green aviation at timeframe 2020-2025. The new configuration without vertical stabilizer named BWB-300 featured with an innovative ship-shaped body was conceived to resolve the requirement of evacuation and to improve passenger experience by providing windows on both sides, as shown in Figure 1(b). Meanwhile the reconciling of the low-speed and high-speed performances was concentrated on. Low-speed wind-tunnel experiments was performed to validate the low-speed aerodynamic design, as shown in Figure 2(a). The high-speed characteristics were studied by using computational fluid dynamics (CFD) method [12].

To further improve the concept for potential applications, it was decided to increase the payload and the cruise Mach number and to keep some experienced design principles on the blending of wing and body [13]-[16]. The centerbody was enlarged for longitudinal control authority and a twin of vertical tails was adopted for providing directional static stability and control. The final configuration for experiments was BWB-330, as shown Figure 1(c). The low-speed tests of configurations with flow-through nacelle (FTN) and turbine-powered simulator (TPS) were conducted in the industrial wind-tunnels, as shown in Figure 2(b). High-speed wind tunnel test was also performed, as shown in Figure 2(c). Consequently, the low-speed and high-speed designs were thoroughly scrutinized and validated.

(a) BWB-300 model (b) Low-speed BWB-330 model (c) High-speed BWB-330 model

Figure 2 Low-/high-speed wind tunnel models of BWB configurations

The objective of present work is to report the progress of the developments on critical technologies of BWB aircraft, including multidisciplinary design and optimization (MDO), stability and control (SC), propulsion and airframe integration (PAI), noise shielding of the centerbody, cabin arrangements and egress evaluation, wind-tunnel experiments and modeling flight test.

2. Developments on Critical Technologies

2.1 Multidisciplinary Design and Optimization

Because of the unique geometry feature that the lifting body, wing, control surfaces and engines are highly integrated, the aerodynamics, structure and stability and control issues are highly interrelated.

BWB has an inherent multidisciplinary integration and appears as a MDO problem. Several MDO works were reviewed by Okonkwo and Smith [17], which emphasized that the optimization should be performed using handling and ride quality as objective functions under the constraints on operating cost and noise. From the perspective of aircraft level, the optimization should include the ultimate performance objectives. However, there are large technology uncertainties during the concept design stage, like the structure and weight due to the noncircular pressurized cabin. Thus most of the conceptual design focus on the high-speed aerodynamic optimization under specified planform and engine technologies.

In NPU two stages of optimization were utilized. In the first stage the cruise aerodynamic efficiency was studied using a two-step optimization framework [12]. The first step was a planform optimization which adopts low-fidelity aerodynamic analysis modules. In the second step a direct iterative surface curvature (DISC) method coupled with a Reynolds-Averaged Navier-Stokes (RANS) based solver was used for the inverse design. During the optimization to resolve the emergency evacuation requirements, a ship-shaped body was kept. The BWB-300 configuration was a detailed practice of this design procedure.

In the second stage, a MDO framework was built with the take-off weight and cruise efficiency as the objective functions under the constrains of longitudinal stability, fuel volume, cabin area, wing span and engine technology [13]-[15]. In this framework, the planform was parameterized which can sweep a large design space. However, due to the computational cost of the RANS solver, a quasi-3D physical based low-fidelity aerodynamic module was adopted. The effects of longitudinal static stability margin and thrust specific fuel consumption (TSFC) on the BWB planform were studied [15]. It was found that the stability was mainly adjusted by the wing position and sweep, as expected. A very stable design having the stability margin compared with conventional TAW configuration exhibits very backwards wing position. The TSFC also has a strong effect on the planform but has a saturation trend when the TSFC reaches a 20% improvement compared with state-of-art of engine technology. Meanwhile the most aerodynamic efficient design all featured a slimmer body to wave wing span for the wing.

During the conceptual design a thoroughly low-and high-speed trade-off design was performed [18]. A leading-edge slotted Krueger flap combining with a single-hinged trailing-edge flap were designed as high-lift devices [19]. To facilitate the trim penalty on cruise efficiency and take-off longitudinal control requirements, a positive stability margin of 0.05 was chosen. To increase the efficiency of elevons, the centerbody length was enlarged. To realize the directional static stability a twin of vertical stabilizer was designed. The final configuration was BWB-330, as shown in Figure 1(c), and the design parameters are given in Table 2.

Table 2 Design parameters of BWB-330

W_{TO} [kg]	b [m]	L [m]	S_{ref} [m2]	C_{ref} [m]	*Altitude* [km]	C_L	C_L/C_D
235,308	70.8	45	942	26.2	12	0.25	24

2.2 Stability and Control Design

2.2.1 Control surface layout and design

During the development of BWB, the SC design exhibited as a challenge, which is related to the high control power, low longitudinal and lateral stabilities, as well as small natural yaw damping. The static stability and control are strongly interrelated and conflict with one another. The degree of stability determines the magnitude of the control action. The right amount of both stability and control has to be found. The degree of static stability selection depends on the design philosophy and the use of stability augmentation with active controls.

A positive zero-lifting moment coefficient with positive stability margin was realized in our final MDO design, which achieves a naturally trimmed design at the design lift coefficient and maximum lift-to-drag ratio during the cruise. It was proved that a balanced and stabilized design could be achieved through profile camber or wingtip twisting combining with sweep.

Control surface sizing is a key challenge for BWB design, mainly due to unconventional flight dynamics connected with multiple redundant control surfaces. The control surfaces layout was decided on the requirements of high-lift, pitch, yaw, roll and drag controls. A system of trailing edge elevons used for flight control is an obvious common feature, which is justified by their short moment arms and low individual control authority. An individual traditional horizontal stabilizer is not required as a relaxed longitudinal stability is adopted compared with TAW. However, a twin of inclined vertical stabilizers and the corresponding control surfaces are adopted to enhance the directional stability and control, which resembles most of recently studied concepts. It was found that the directional stability and control is not enough if only the winglets and split drag rudders were adopted.

The control surface sizing not only needs to satisfy the control authority requirements but also needs to provide good handling qualities for civil aircraft. The sizing of the elevons was realized using the stability and control module in the MDO framework during the planform optimization under the constraints on the requirements of take-off rotation. The conventional volume coefficient method was used to size the twin inclined stabilizers under the constraints on one engine out and crosswind landing trim requirements. The final control surface layout is shown in Figure 3.

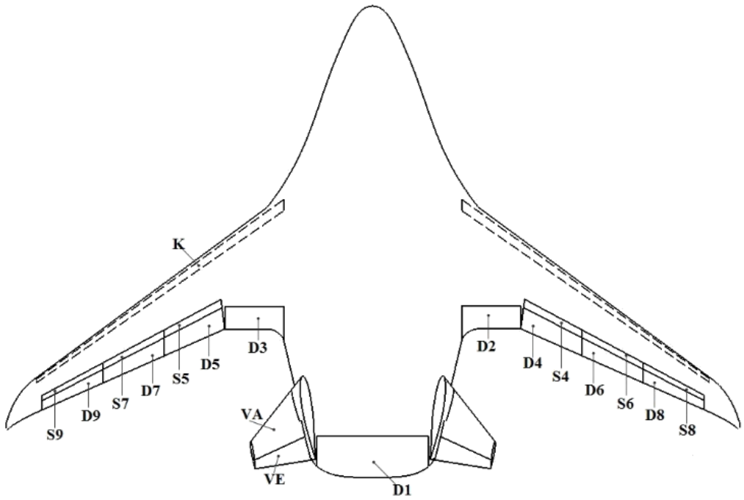

Figure 3 The control surface layout of BWB-330

The leading-edge Krueger flaps (K) combing trailing-edge simple single-hinged flap (D2-D5) are used as high-lift devices without severe pitching-down moments. The pitch control is provided by simply hinged elevons at the trailing edge of the centerbody (D1) combining symmetrically deflected inclined rudder (VE). The yaw control is provided by the inclined rudders (VE). Additional yaw control is realized by the outboard combined control surfaces (S8/D8 and S9/D9). The thrust vectoring or the rudders on the winglets is not adopted. The roll control is provided by asymmetrical deflection of the trailing edge elevons on each outboard wing (D6-D9). All the spoilers (S4-S9) can be effectively used for load alleviation, high-lift enhancing or combining with other control surfaces for drag controls.

A series of CFD and wind-tunnel tests has been conducted to obtain an aerodynamic database after the stabilizer and control surface sizing, which is used to evaluate the open-loop SC characteristics the conceptual configuration and to design the closed-loop control laws.

2.2.2 Static stability and control derivatives

The linearized flight dynamic equations are used to study the essential SC characteristics of the BWB-330 in the flight profile. The static stabilities of four traditional flight states are shown in Table 3. The longitudinal stability is small compared with conventional TAW as designed. The lateral stability is comparable with that of TAW at cruise states but is large at take-off and landing states The directional stability is positive but is quite less than that of TAW. The lateral and directional stabilities are all smaller than -0.057 and 0.057 recommended by Donlan for flying wing [20].

Table 3 The static stability and damping derivatives of BWB-330

Flight state	K_n [%]	Cl_β	Cn_β	Cm_q	Cl_p	Cn_r
TF*	4.3	-0.090	0.031	-0.56	-1.39	-0.029
LD	6.8	-0.066	0.031	-0.56	-1.39	-0.029
CRL	5.2	-0.153	0.017	-0.30	-1.09	-0.035
CRH	5.3	-0.173	0.011	-0.30	-1.09	-0.035

*TF - Take-off, LD – Landing, CRL – Low-speed low altitude cruise, CRH- High-speed cruise

Due to the small body-length of BWB, the damping effects of centerbody is weak. Hence the longitudinal damping derivatives are quite less than that of TAW. However, the wide blended wing and body is preferred for lateral damping. The lateral damping derivatives are almost three times of that for TAW. The directional derivative is about one tenth of that for TAW due to the small area of vertical tail and the small body length. The control derivatives are also evaluated. As the lever arm is short, the pitching control derivatives of elevons are about one twentieth of that for TAW. The rolling control derivatives are comparable with that of TAW. The directional control derivatives are just one fifth to half of that for TAW.

2.2.3 Dynamic stability

The eigenvalue, nature frequency, period and damping ratio of short period mode and phugoid mode for longitudinal dynamic stability characteristics are shown in Table 4. The longitudinal motion is dynamically stable. The period of short period mode is in the range of 1-2 seconds for different flight states. However, the period of phugoid mode is quite different foe different flight conditions. The damping ratio is quite reasonable compared with other BWB configurations.

Table 4 The longitudinal dynamic stability characteristics of BWB-330

Flight state	Mode	Eigenvalue	ω_n (rad/s)	T (s)	ζ
TF	SP	-0.6786 ± 0.9371i	1.16	1.5	0.59
	PH	-0.0078 ± 0.1498i	0.15	128.0	0.05
LD	SP	-0.8676 ± 1.3102i	1.57	1.2	0.55
	PH	-0.0106 ± 0.1541i	0.16	94.1	0.07
CRL	SP	-0.5907 ± 1.4116i	1.53	1.7	0.39
	PH	-0.0012 ± 0.1006i	0.10	825.0	0.01
CRH	SP	-0.8043 ± 2.8253i	2.94	1.2	0.27
	PH	-0.0020 ± 0.0538i	0.05	491.0	0.04

The eigenvalue, nature frequency, period and damping ratio of roll (R), Dutch roll (DR) and spiral modes for lateral-directional dynamic stability characteristics are shown in Table 5. The characteristics of roll mode are quite good, but the frequency and damping of Dutch mode are quite small. All the spiral modes are stable.

Table 5 The lateral-directional dynamic stability characteristics of BWB-330

Flight state	Mode	Eigenvalue	ω_n (rad/s)	T (s)	ζ
	Roll	-6.8577	6.9	0.2	1.0
TF	DR	-0.0683±0.4823i	0.49	14.6	0.14
	Spiral	-0.0082	0.01	122.0	1.0
	Roll	-11.7570	11.8	0.1	1.0
LD	DR	-0.0996±0.5651i	0.57	10.0	0.17
	Spiral	-0.0060	0.01	165.0	1.0
	Roll	-7.3041	7.3	0.1	1.0
CRL	DR	-0.1007±0.5428i	0.55	9.9	0.18
	Spiral	-0.0186	0.02	53.7	1.0
	Roll	-6.4476	6.45	0.2	1.0
CRH	DR	-0.0833±0.5554i	0.56	12.0	0.15
	Spiral	-0.0176	0.02	56.7	1.0

2.2.4 Flying and handling quality

Based on the criterions of standards MIL-STD-1797A and MIL-F-8785C, the open-loop flying and handling qualities are analyzed. From the Table 4 it can be seen that all the flight states can satisfy the Level 1 requirements except CRH that can reach Level 2 for short period modes. For phugoid mode Level 1 is satisfied for all flight states except CRL which can just satisfy Level 2. For the lateral-directional dynamic modes, all roll modes can satisfy the requirements of Level 1. Only the Dutch roll mode of LD can achieve Level. Other modes can just satisfy the requirements of Level 2. As the eigenvalue of spiral modes are negative, all the spiral modes achieve Level 1 flying quality. Based on the above analysis, a stability augmentation system (SAS) is required to obtain better SC and flying qualities. All the flying and handling qualities achieve Level 1 after adopting SAS.

2.3 Propulsion and aircraft integration

The fuel efficiency is a driven design matrix for BWB development, which can be an important determinant of aircraft range, size, economics, noise and emissions. However, quite conventional engine technologies were adopted for BWB-330, which are similar to GENx. At the top of climb, the overall pressure ratio is 60; the fan pressure ratio is 1.5 and the bypass ratio is 9.3. The TSFC is 0.53 $lb \cdot lbf^{-1} \cdot h^{-1}$. The resulting thrust-to-weight ratio is 0.25.

The configuration of BWB opens new opportunity of propulsion and airframe integration (PAI), which can result in system benefits of fuel efficiency and noise reduction, but also consequent challenges. A variety of propulsion options, including embedded engines, podded engines in nacelles, direct-drive turbofans, geared turbofans and open rotors have been investigated for BWB. The mounting positions can also be quite different, including conventional under-wing, aft-upper surface of centerbody, upper wing trailing edge, embedded in the body with BLI and distributed along the span. To reduce the risk for near term application, the podded engines in nacelle mounted on the aft-upper centerbody was adopted to provide better noise shielding effects, which is the most used concept.

The integration of engines on the pylons near the trailing edge of upper surface is quite challenging. The interferences between the propulsion and airframe can be quite complex. The engines are in local high-speed flow on the centerbody upper surface, which leads to appearance of strong shocks over the nacelles and corresponding flow separations. The resulting airframe drag can be high. At high angle of attack or high sideslip angle, the inlet flow of engines can be highly distorted, which can result in fan flow instability and propulsive efficiency reduction.

To address the specific PAI challenges, thorough numerical and wind tunnel studies were carried out. A powered nacelle was optimized to weaken the compressibility effects at cruise condition under the constraints on low-speed off-design conditions [21]. The maximum Mach number over the nacelle is effectively reduced. A parametric integration design method was proposed to perform the detailed outer mold line design of the centerbody [16]. The avoiding of the throat effect formed by the nacelle, pylon and airframe is realized. The supersonic regions around the nacelle are effectively reduced, concentrating mainly on the lip position. Therefore, the strong shock waves and the related flow separation can be successfully eliminated. A significant cruise-drag reduction is achieved.

Meanwhile, the effects of engine intake and exhaust on the aerodynamic performance at cruise were numerically studied [22]. And the install effects on thrust were also investigated in detail [23]. Due to the unconventional position of the engine, the thrust reverser cascade feasibility was also preliminarily evaluated [24].

2.4 Noise Shielding Effects

Noise reduction is an obligation for future civil aviation reflected on the more stringent noise regulation. BWB has specific noise features due to its unconventional configuration and performance. BWB has inherent features with aft upper centerbody mounted engines, low-wing loading and simple-hinged trailing edge flap, which can help noise reduction. The distinct characteristics of airframe noise related to the slotted Krueger and landing gears were reviewed in reference [3].

The interactions of propulsion and airframe aeroacoustics (PAA) are quite different with that of conventional TAW with under wing mounted engines. It is favorable to adopt ultra-high bypass-ratio engines when they are mounted on the aft upper rear centerbody. Meanwhile the upstream propagating noise can be effectively shielded by the wide centerbody. The distance of the engine exhauster to the trailing edge of the centerbody and the features of noise sources, such as spectra and directivity, are the dominant parameters of PAA effects.

Because there is historical database on the shielding and it is very expensive to directly model these effects using high-fidelity computational aeroacoustics methods. A simplified experiment was adopted to investigate the shielding effects. The experiments have been done in the anechoic noise calibration facility of AVIC aerodynamics research institute, as shown in Figure 4. The anechoic chamber has a length of 6.0 m, a width of 5.2 m, a height of 4.9 m. The cut-off frequency is 200 Hz.

In the experiments, a simplified BWB model is obtained by the projection of the model in the horizontal plane. The experimental model has a ratio of 1:33.22 to the original scale, an area of 0.725 m^2, a span of 1.9m and a body length of 1.23m. When the centerbody tip is used as the origin of the coordinate, the center of the gravity is located at (730.36 mm, 0 mm, 0 mm). The noise source is located at (976.22 mm, 120.365 mm, 120.365 mm).

Figure 4 The sketch of the model mounted in the anechoic chamber

A circle microphone array of the anechoic noise calibration facility has a diameter of 2m. There are 36 microphones distributing uniformly on the circle microphone array. The circle of the array can move back and forth on the tracks having a step of 10 cm with a maximum distance of 230 cm. A data acquisition system based on PXIe bus was used, which is composed by a series of multi-channel data acquisition card. The sampling frequency can be as high as 200kHz. In the experiment, the sampling frequency is 40960 Hz. The data block number is 100 with 2048 data points in each block.

A point noise source is designed with the directivity like that of the monopole source, having a rated power of 60 W, sound pressure level (SPL) of 93 dB, and a frequency range from 400 Hz to 10 kHz. The fast Fourier transformation (FFT) is used to analyze the one-third octave spectra and total SPL of the data from each tunnel. The total SPL and SPL at different frequencies are drown along the longitudinal direction as horizontal axis (with an interval of 10 cm) and in circumference (from 0° to 360°) direction.

The total SPL distribution around the BWB model is shown Figure 5. Without the BWB model, the SPL is slightly higher in the region $x = 80 - 150cm$ and angle $\phi = 0° - 200°$, as shown in Figure 5(a), due to the point source is not at the exact center of the measuring ring. When the BWB model is installed, the total SPL is shown in Figure 5(b), which increases in the region $\phi = 90° - 270°$ along the longitudinal direction, due to the reflection of the BWB upper surface. The shielding effect is obvious in the region $\phi = 280° \sim 80°$ along the longitudinal direction at almost all measure positions. The total SPL difference with and without BWB model is shown in Figure 5(c), where the positive value indicates SPL increasing and the negative values indicates SPL decreasing. The maximum shielding effects can be as high as 10 dB.

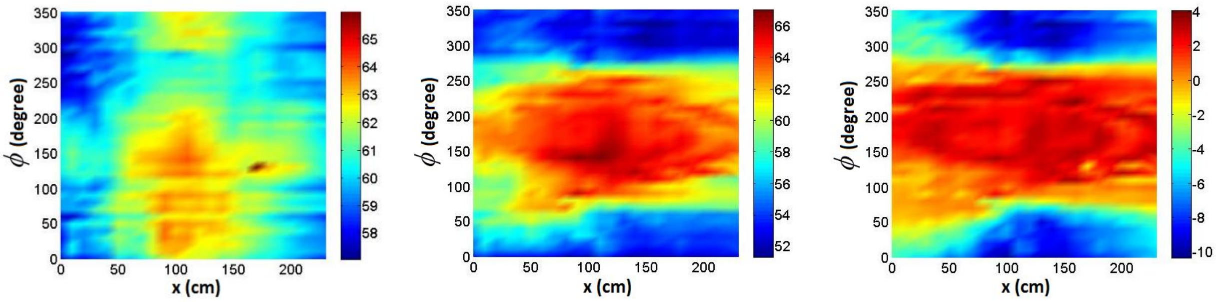

(a) Without BWB model (b) With BWB model (c) The difference

Figure 5 Comparisons of total SPL without/with BWB model and the shielding effect

To know the influence of frequency on the shielding effects, the one-third octaves of SPL difference at different center frequencies are shown in Figure 6. When the frequency is low, the insertion loss due to the presence of the body is small (-2dB~-6dB). When the frequency increases, the insertion loss increases to (-10dB~-15dB). This is because the low-frequency noise has large wavelength. When the wavelength is larger than or equivalent to the model size, the sound wave is diffracted.

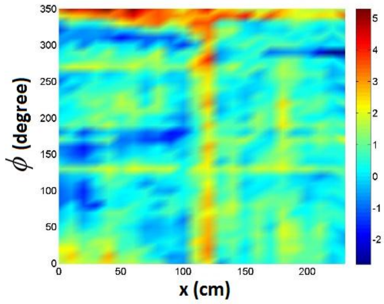

(a) f=400Hz

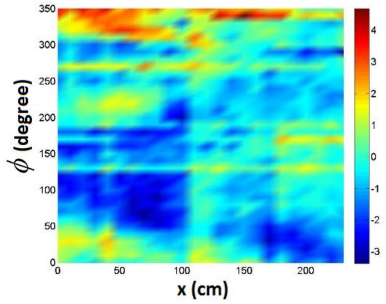

(b) f=500Hz

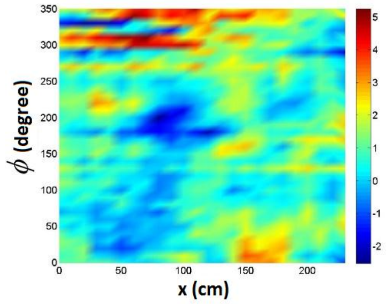

(c) f=630Hz

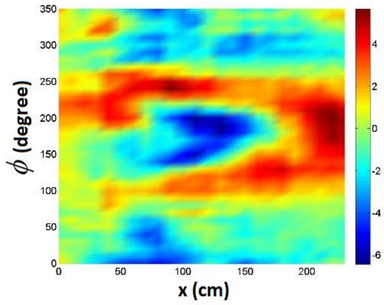

(d) f=800Hz

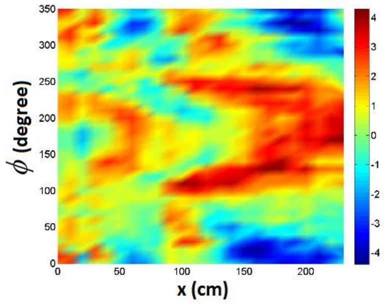

(e) f=1000Hz

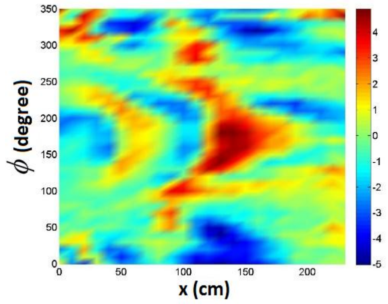

(f) f=1250Hz

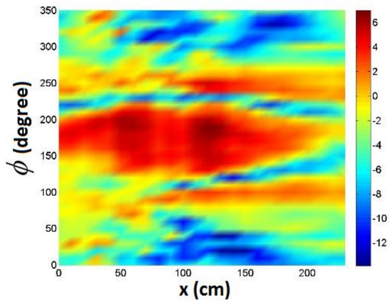

(g) f=1600Hz

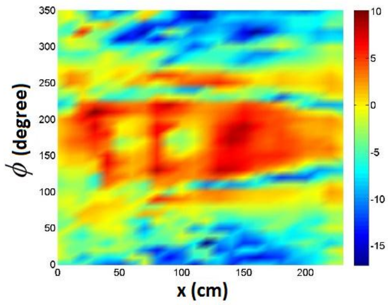

(h) f=2000Hz

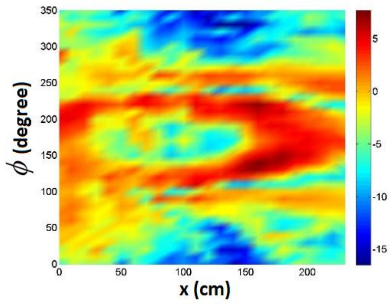

(i) f=2500Hz

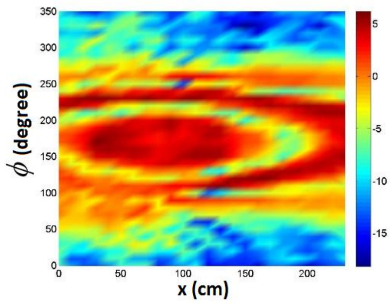

(j) f=3150Hz

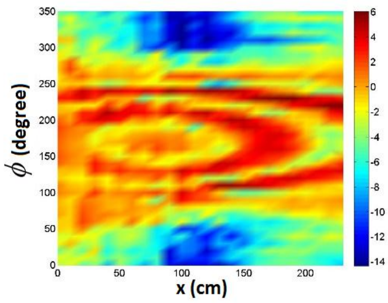

(k) f=4000Hz

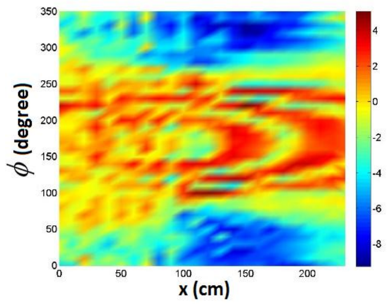

(l) f=5000Hz

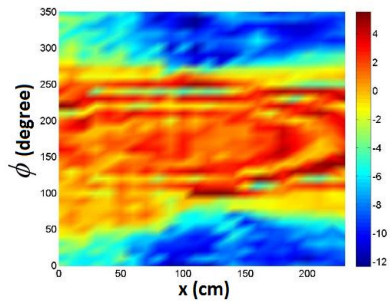

(m) f=6300Hz

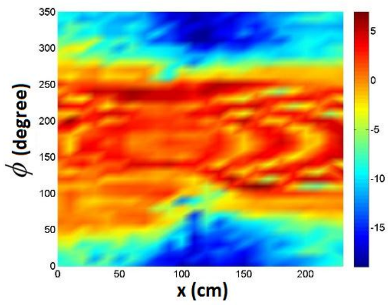

(n) f=8000Hz

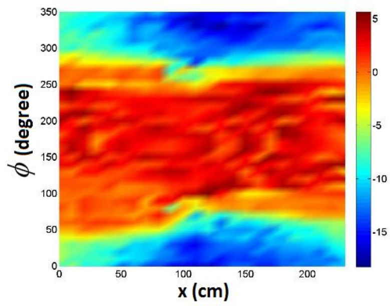

(o) f=10000Hz

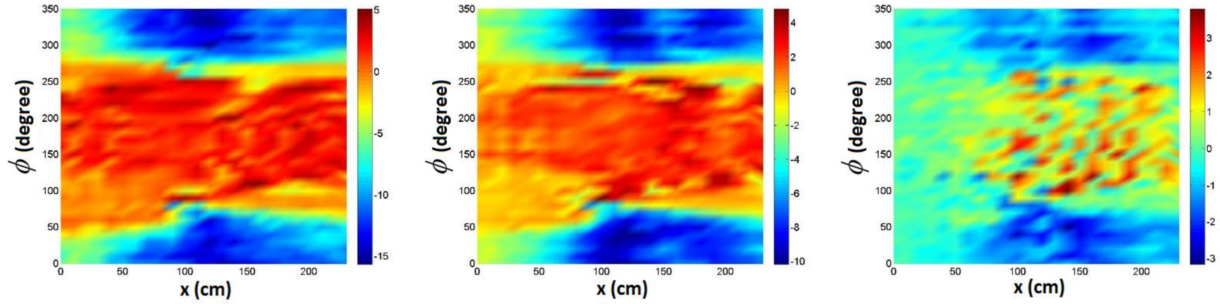

(p) f=12500Hz (q) f=16000Hz (r) f=20000Hz

Figure 6 The one-third octaves of SPL-difference for white point source at different center frequencies

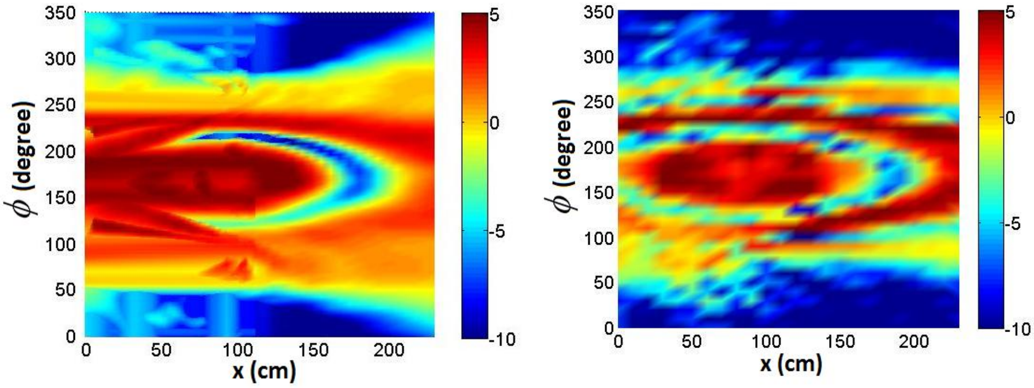

(a) Numerical result (b) Experimental data

Figure 7 Comparisons of computational and experimental SPL-difference at 3150 Hz

A numerical method based on equivalent source method was also developed to predict the shielding effects, which is validated against the experimental data, as shown in Figure 7. The SPL differences and the shielding pattern are predicted well. The differences between the computational and experimental results would be due to the limited resolution in the experiments.

2.5 Cabin Arrangements and Egress Evaluation

A main difference between the BWB-330 to other BWB concepts is the cabin arrangement due to its slim centerbody and extended body length. The multi-functional, three-class and economical interior arrangements are shown in Figure 8. The maximum number of seats in a line is 16, which is quite less than that of VELA-1 (32 seats in a line) [25] and BWB-450 (29 seats in a line) [2]. There are eight Type-A emergency exits that are on both sides of the centerbody, which is much less than 20 exits around VELA-1, and 22 exits at front and rear of the centerbody for BWB-450.

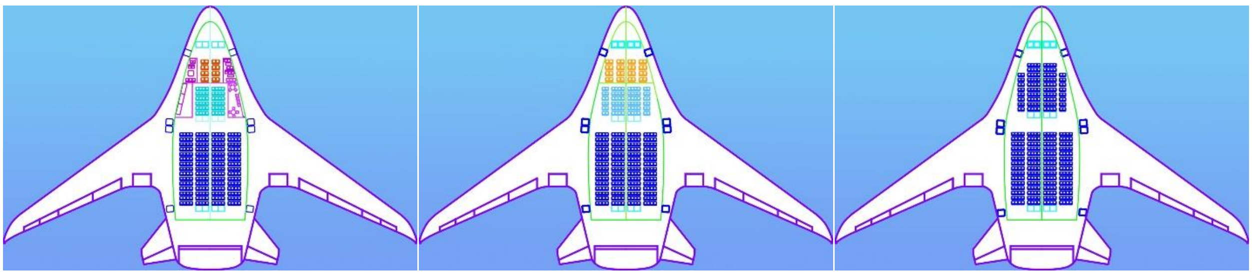

(a) Multi-functional (b) Three-class (c) Economical

Figure 8 Cabin arrangements for BWB-330 with different seats

An evacuation simulation software based on the coupling of cellular automata and multi-agent system was used to evaluate the egress time. One thousand simulations were performed for each egress condition. When the both-side exits are open, the predicted results are shown in Table 6. When only one-side exits are available, the predicted results are shown in Table 7, which is quite less than that of VELA-1 [25]. All the predicted data satisfy the airworthiness regulations.

Table 6 The egress prediction for all exits open

Predicted data	TET(s)	PET(s)	FOT(s)	OPS
Maximum	59.52	39.71	14.96	0.3124
Minimum	50.36	26.53	12.34	0.0367
Average	55.07	36.71	13.17	0.1066
Standard deviation	1.4818	0.8988	0.4071	0.0376

TET=total egress time, PET=Personal egress time, FOT= first operation time, OPS=operates per second

Table 7 The egress prediction for one-side exits open

Predicted data	TET(s)	PET(s)	FOT(s)	OPS
Maximum	83.03	37.90	15.52	0.4244
Minimum	64.39	33.14	13.81	0.2156
Average	72.62	35.05	14.54	0.3291
Standard deviation	3.3003	0.9013	0.3576	0.0363

2.6 Wind Tunnel Experiments

To validate the design methods and to obtain the fundamental aerodynamic performance, the low-speed and high-speed ground tests were performed in AVIC large-scale production wind tunnels. The steel models were designed and fabricated by AVIC Huiyang aviation propeller company.

2.6.1 Low-speed wind tunnel experiments

The low-speed model has a scaling ratio of 1/22.4 and has been tested in two low-speed wind tunnels. One is FL-51 of test cross-section 4.5m×3.5m×10m, as shown in Figure 2(b). The flow speed is 70m/s at Reynolds number 5.0×10^{6} based on the mean aerodynamic chord. The other is a pressurized tunnel FL-9 having the same cross-section as FL-51 to investigate the effects of Reynolds number at 1.0×10^{7} and 2.0×10^{7}. Besides the aerodynamic force measurements, the fluorescence tuft flow visualization was also adopted to observe the flow separation. To study the effects of engines' inlet flow and exhaust, two ejected-powered-engine simulators (EPES) were adopted with the bypass pressure ratio 1.54 and inner pressure ratio 1.22, as shown in Figure 9.

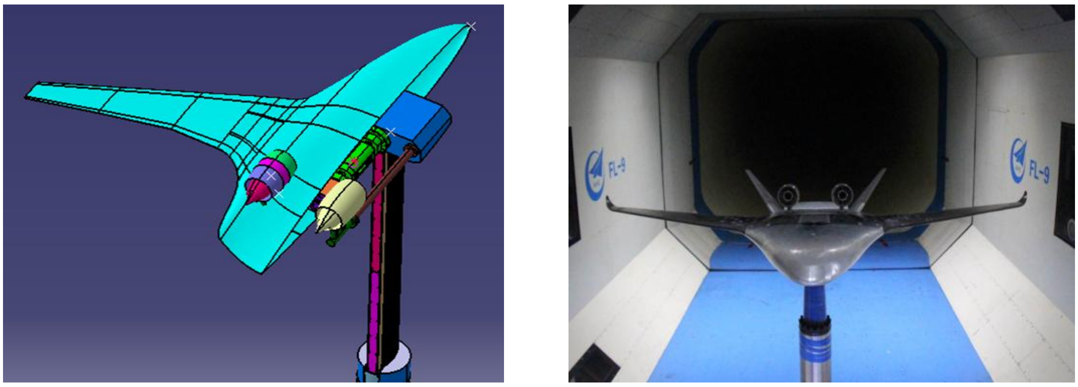

(a) The sketch of the EPES (b) Low-speed BWB with EPES in FL-9

Figure 9 Low-speed BWB model with EPES

The low-speed CFD results were compared with the wind-tunnel results at the test condition, as shown in Figure 10(a). The CFD tools can predict the basic aerodynamic forces well. The effects of EPES on the lift, drag and pitching moment are shown in Figure 10(b). The lift and pitching-down moments are increased, but the drag does not change till moderate lift.

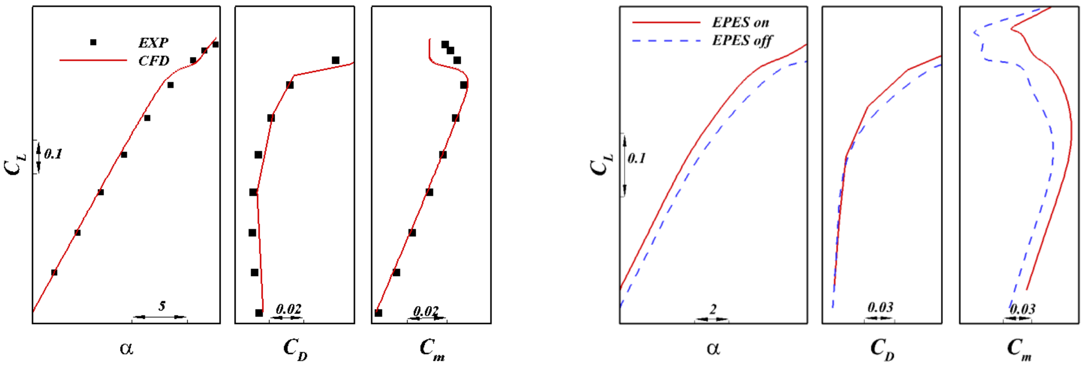

(a) Comparisons of CFD and test results (b) Effects of EPES on aerodynamic forces

Figure 10 Low-speed experimental results without and with EPES

2.6.2 High-speed wind tunnel experiments

The high-speed model has a scaling ratio of 1/72, and the FL-3 wind tunnel of AVIC was used,which has a test cross-section of 4.2m×1.5m×1.6m, as shown in Figure 2(c). Besides the aerodynamic force measurements, the surface oil-flow visualization and the pressure sensitive paint (PSP) were also adopted to analyze the surface flow topology and to validate CFD tools. The CFD results of force coefficients and surface pressure coefficient distribution are compared with that of experiments, as shown in Figure 11. The CFD can predict quite reasonable results.

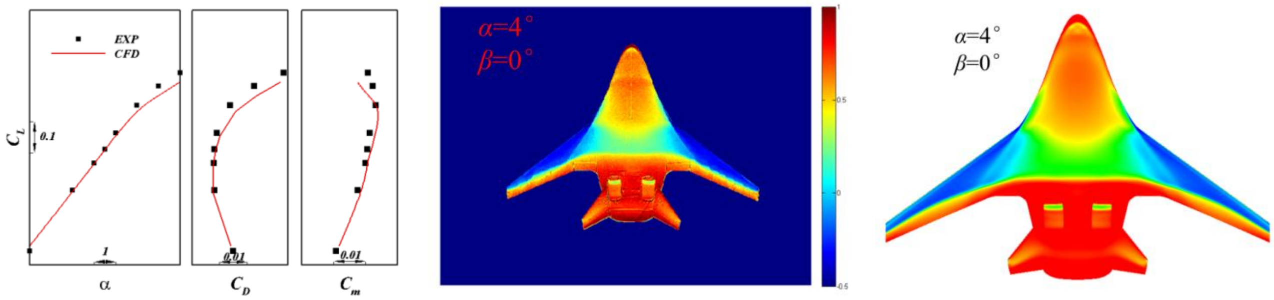

(a) Force coefficients (b) Experimental Cp using PSP (c) Computational Cp

Figure 11 Comparisons of CFD and high-speed experimental results at Ma=0.85, Re=7.2×10^6

2.7 Modeling Flight Test

Using the appropriate editor each equation should occur on a new line with uniform spacing from

To know the dynamic characteristics of continuous flight motions of BWB, a modeling fight test were executed. The objectives are to thoroughly know the fundamental low-speed characteristics of take-off, landing and SC. The modeling BWB aircraft has a scaling ratio of 1/9.85, is designed according to dynamical scaling laws and cruises at altitude of 3000 m for 30 minutes. The take-off weight is 230 kg.

(a) Structral design (b) The first model aircraft

Figure 12 The structure design and the first model aircraft

The model aircraft is a little bit larger than X-48B [26] and is almost two times of recently reported MAVERIC of airbus. Three models will be constructed. Each model has a cruise configuration and a high-lift configuration with Krueger flap. The structure design and the first aircraft are shown in Figure 12. The flight tests will be carried out in this year.

3. Summary and Further Developments

In the last decade, large progress on the development next generation civil aircraft has been made around the world, specifically on the blended-wing-body aircraft development. A persistent effort has been performed in the last decade in Northwestern Polytechnical University and is summarized in the present paper, which includes multidisciplinary optimization and design, stability and control design, propulsion and airframe integration, the noise shielding effects, cabin arrangements and egress, wind-tunnel experiments and modeling flight tests. From these efforts supported by the institutes and companies, it can be found that a stable, high efficient, and safe design can be realized. However, much more work have to be done on the structure design and high-speed modeling flight test.

4. Contact Author Email Address

zhenlichen@nwpu.edu.cn

5. Copyright Statement

Acknowledgements

This work was supported partially by the Fundamental Research Funds for the Central Universities (Nos. 3102019JC009 and G2016KY0002).

References

[1] Green JE. Greener by design - the technology challenge. *Aeronautical Journal*,Vol.106, No.1056, pp 57-103,2002.

[2] Liebeck RH. Design of the Blended-Wing-Body subsonic transport. *Journal of Aircraft*, Vol. 41, No. 1, pp 10-25, 2004.

[3] Chen ZL, Zhang MH, Chen YC, Sang WM, Tan ZG, Li D and Zhang BQ. Assessment on key enabling technologies of hybrid-wing-body civil transport. *Chinese Journal of Aeronautics*, Vol. 32, No. 8, pp 1797-1827, 2019.

[4] Bonet JT, Schellenger HG, Rawdon BK, Elmer KR, Wakayama SR, Brown DL, Guo YP. Environmentally responsible aviation (ERA) project-N+2 advanced vehicle concepts study and conceptual design of subscale test vehicle (STV)-final report. *NASA Dryden Flight Research Center*, Report No.: NASA/CR-2011-216519, 2011.

[5] Zhang BQ, Chen ZL, Li J. The trend of aerodynamic configuration development in large subsonic transport aircraft. The key technology of large aircraft forum. *Chinese Society of Aeronautics and Astronautics*, Shenzhen, pp 1-6, 2007 (in Chinese).

[6] Zhu ZQ, Wang XL, Wu ZC, et al. A new type of transport-blended wing body aircraft. *Acta Aeronautica et Astronautica Sinica,* Vol. 29, No. 1, pp 49-59, 2008 (in Chinese).

[7] Zhu ZQ, Wang XL, Wu ZC, et al. Discussion of design methods for silent and fuel efficient medium range civil transport. *Acta Aeronautica et Astronautica Sinica*, Vol. 29, No. 3, pp 562-572, 2008 (in Chinese).

[8] Liao HJ, Zhang SG. Design of cabin layout for blended wing body passenger transports. *Journal of Beijing University of Aeronautics and Astronautics,* Vol. 35, No. 8, pp 986-989, 2009 (in Chinese).

[9] Zhang SG, Lu YH, Gong L, et al. Research on design of stability and control of a 250-seat tailless blended-wing-body civil transport aircraft. *Acta Aeronautica et Astronautica Sinica*, Vol. 32, No. 10, pp 1761-1769, 2011 (in Chinese).

[10]Zhao ZG, Zhang SG. Analysis of effects of BWB airliner design parameters on its economic profitability. *Journal of Beijing University of Aeronautics and Astronautics*, Vol. 37, No. 8, pp 937-942, 2011 (in Chinese).

[11]Jiang J, Zhong BW, Fu S. Influence of overall configuration parameters on aerodynamic characteristics of a blended-wing-body aircraft. *Acta Aeronautica et Astronautica Sinica*, Vol. 37, No. 1, pp 278-289, 2015 (in Chinese).

[12]Li PF, Zhang BQ, Chen YC, Lin Y. Aerodynamic design methodology for blended wing body transport. *Chinese Journal of Aeronautics*, Vol. 25, No. 4, pp 508-516, 2012.

[13]Zhang MH, Chen ZL and Zhang BQ. A conceptual design platform for blended wing-body transports. *30th Congress of the International Council of the Aeronautical Science*, Daejeon, 2016-0510, 2016.

[14]Gu WT, Chen ZL and Zhang BQ. Physically-based multidisciplinary design optimization framework coupling airframe and propulsion. *30th Congress of the International Council of the Aeronautical Science,* Daejeon, 2016-0268, 2016.

[15]Zhang MH, Chen ZL, Tan ZG, Gu WT, Li D, Yuan CS and Zhang BQ. Effects of stability margin and thrust specific fuel consumption constrains on multi-disciplinary optimization for blended-wing-body design Multi-disciplinary design of a practical Blended-Wing-Body commercial aircraft. *Chinese Journal of Aeronautics*, Vol. 32, No. 8, pp 1847–1859, 2019.

[16]Xin ZQ, Chen ZL, Gu WT, et al. Nacelle-airframe integration design method for Blended Wing Body transport with podded engines. *Chinese Journal of Aeronautics*, Vol. 32, No. 8, pp 1860–1868, 2019.

[17]Okonkwo P, Smith H. Review of evolving trends in blended wing body aircraft design. *Progress in Aerospace Sciences*, Vol. 82, pp 1–23, 2016.

[18]Zhang MH, Chen ZL, Gu WT, Li D, Zhang S, Yuan CS, Wang L and Zhang BQ. Tradeoff design of high and low speed performance for blended-wing-body civil aircraft. *Acta Aeronautica et Astronautica Sinica,* Vol. 40, No. 9, 623052, 2019 (in Chinese).

[19]Zhang MH, Chen ZL, Mao J, Wang G, Tan ZG, Wang L and Zhang BQ. Design of Krueger flap for civil aircraft with blended-wing-body. *Acta Aeronautica et Astronautica Sinica*. Vol. 40, No. 9, 624048, 2019 (in Chinese).

[20]Donlan CJ. An interim report on the stability and control of tailless airplanes. *Langley Field: NACA Langley Aeronautical Lab*, Report No.: NACA/TR-796, 1944.

[21]Gu WT, Zhao ZS, Zhou HW, Feng J, Tan ZG and Li D. Powered-on nacelle design on blended wing body configuration with podded engines. *Acta Aeronautica et Astronautica Sinica*. Vol. 40, No. 9, 623047, 2019 (in Chinese).

[22]Gu WT, Chen YC, Xin ZQ, Chen ZL and Zhang BQ. Intake and exhaust effect on aerodynamic characteristics of blended wing body civil aircraft with podded engines. *Journal of Aerospace Power*, Vol.34, No. 6, pp 1297-1310, 2019 (in Chinese).

[23]Gu WT, Chen YC, Chen ZL, Sang WM and Zhang BQ. Investigation of engine installed effects on thrust of blended wing body transport with podded engines. *Journal of Propulsion Technology*, Vol.41, No. 2, pp 260-267, 2020 (in Chinese).

[24]Yu G, Li D, Chen ZL and Zhang ZY. Blended wing body thrust reverser cascade feasibility evaluation through CFD. *IEEE Access*, Vol. 7, pp 155184-155193, 2019.

[25]Galea ER, Filippidis L, Wang Z and Ewer J. Fire and evacuation analysis in BWB aircraft configurations: computer simulations and large-scale evacuation experiment. *The Aeronautical Journal*, Vol. 114, No. 1154, pp 271-277, 2010.

[26]Vicroy DD. Blended-Wing-Body Low-Speed Flight Dynamics: Summary of Ground Tests and Sample Results (Invited). *47th AIAA Aerospace Sciences Meeting Including The New Horizons Forum and Aerospace Exposition*, Orlando, Florida, AIAA 2009-933, 2009.